PTEP

Prog. Theor. Exp. Phys. **2024** 123B03 (12 pages)
DOI: 10.1093/ptep/ptae169

Warm Surprises from Cold Duets: *N*-Body Simulations with Two-Component Dark Matter

Jeong Han Kim[1], Kyoungchul Kong[2], Se Hwan Lim[1], and Jong-Chul Park[3,*]

[1]*Department of Physics, Chungbuk National University, Cheongju, Chungbuk 28644, Republic of Korea*
[2]*Department of Physics and Astronomy, University of Kansas, Lawrence, KS 66045, USA*
[3]*Department of Physics and IQS, Chungnam National University, Daejeon 34134, Republic of Korea*
*E-mail: jcpark@cnu.ac.kr

Received August 7, 2024; Revised October 14, 2024; Accepted November 1, 2024; Published November 15, 2024

We explore extensive *N*-body simulations with two-component cold dark matter candidates. We delve into the temperature evolution, power spectrum, density perturbation, and maximum circular velocity functions. We find that the substantial mass difference between the two candidates and the annihilation of the heavier components to the lighter ones effectively endow the latter with warm dark matter-like behavior, taking advantage of all distinct features that warm dark matter candidates offer, without observational bounds on the warm dark matter mass. Moreover, we demonstrate that the two-component dark matter model aligns well with observational data, providing valuable insights into where and how to search for the elusive dark matter candidates in terrestrial experiments.

Subject Index B71, B73, E70

1 Introduction

The nature of dark matter (DM) remains mysterious even after decades of a multitude of experiments in particle physics and great advances in observational astrophysics and cosmology [1]. The majority of cosmological simulations focus on a single DM candidate for its simplicity and approximate consistency with much of the observational data, while various theoretical models of dark matter, including multicomponent dark matter [2,3], have been proposed to address some of the unresolved queries and to better understand the data in current and upcoming experiments [4]. Most existing studies on two-component dark matter consider *N*-body simulation with two noninteracting cold dark matter (CDM) components [5] or with noninteracting CDM and warm dark matter (WDM) [6–10]. A nontrivial connection between two-component dark matter and its cosmology has been discussed in the literature, but the model requires an extremely degenerate mass spectrum $\Delta m/m \sim 10^{-8}$ [11–14].

In this paper, we go beyond one single CDM paradigm and perform comprehensive cosmological simulations for two-component CDM candidates with sizable mass splitting and self-interaction (diagram II in Fig. 1) for the light component. After both components decouple from the thermal bath, in addition to the heavy CDM, we expect two types of light CDM to arise: a relic (nonrelativistic) component and boosted DM from the annihilation of the heavy CDM. The light-boosted components share their energy with the slow-relic component, increasing the temperature via sizable nongravitational self-interaction, and therefore making the light relic behave like WDM, as illustrated in Fig. 1. Such a scenario naturally connects between models with two CDM components and models with CDM + WDM. Therefore, this model

Funded by SCOAP[3]

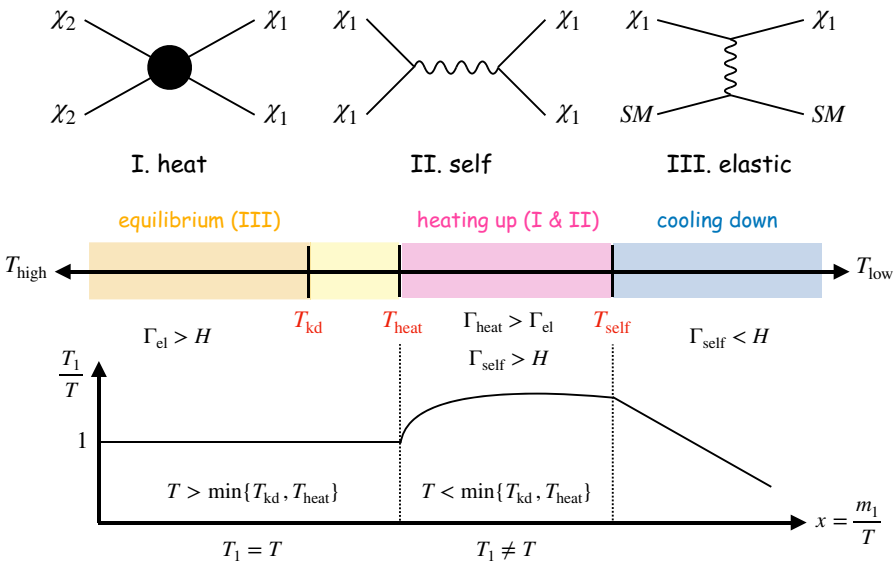

Fig. 1. Brief thermal history of the Universe with two-component CDM. Different stages are defined by three important temperatures, T_{kd}, T_{heat}, and T_{self}, which are determined by the balance between the various interaction rates and the Hubble parameter H: $\Gamma_{el} \leftrightarrow H$, $\Gamma_{el} \leftrightarrow \Gamma_{heat}$, and $\Gamma_{self} \leftrightarrow H$, respectively. Γ_{heat}, Γ_{self}, and Γ_{el} are the interaction rates due to heating process (I), self-interaction (II), and elastic scattering (III), respectively.

innately takes advantage of all the distinct features that WDM offers, such as power spectrum, dark matter density profile, small-scale structures, etc. On the other hand, it suffers less from observational bounds on the WDM mass. For example, the WDM mass bound from Lyman-α observations [15,16] is significantly weakened or negligible in this model. WDM becomes hotter as it gets lighter. However, our model controls such behavior with the relic fraction of the light component to the total DM abundance and mass splitting.

Many direct detection schemes have been proposed targeting sub-MeV DM [17–22], while currently operating experiments are not sensitive to the typical WDM mass [23,24]. However, the boosted property of the light DM component offers great opportunities in particle physics experiments [25–59] and cosmological thermal dynamics [60]. However, few studies on cosmological implications of such boosted DM models have been discussed. In this paper, we will carefully examine the temperature evolution, density perturbation, and N-body simulation of the two-component DM model. We derive the model parameters that are consistent with the maximum circular velocity function (MCVF), which can be studied in current and upcoming particle physics experiments.

2. Model

We consider a two-component DM model with a dark sector consisting of two Dirac fermions χ_1 and χ_2 with mass hierarchy $m_2 > m_1$, whose stability is protected by dark $U(1)' \otimes U(1)''$ gauge symmetries [3]. We assume that both χ_1 and χ_2 are charged under $U(1)''$, while only χ_1 is charged under $U(1)'$. The dark sector is allowed to couple to the standard model (SM) sector only through kinetic mixing between $U(1)'$ and $U(1)_Y$. The mixing between $U(1)''$ and $U(1)_Y$ is doubly suppressed due to a loop factor as well as small kinetic mixing between $U(1)'$ and $U(1)_Y$ [25]. The dark gauge symmetries are assumed to be spontaneously broken, leading to

the dark gauge boson masses $m_{A'}$ and $m_{A''}$, respectively. We are interested in the scenario where dark gauge bosons are heavier than χ_1 and χ_2. In this case, χ_2 is disjunct from the SM particles and annihilates only into χ_1, while χ_1 can directly annihilate into the SM particles.

The heavy species χ_2 is kept to thermal equilibrium with the assistance of the light species χ_1 [3] with a thermally averaged annihilation cross section $\langle\sigma v\rangle_{22\to 11}$, while χ_1 pair-annihilates directly to SM particles with the cross section $\langle\sigma v\rangle_{11\to XX}$, where X stands for SM particles. We assume that χ_1 couples predominantly to electrons for simplicity. Relic abundances of χ_1 and χ_2 are denoted as Ω_1 and Ω_2, respectively, and the total abundance should agree with the observed one, $\Omega_{\rm DM} = \Omega_1 + \Omega_2 \simeq 0.27$. The fraction of χ_1 is expressed by $r_1 = \Omega_1/\Omega_{\rm DM}$. The free parameters of the model are $\{m_1, m_2, m_{A'}, m_{A''}, g', g'', \epsilon\}$, where g' and g'' denote gauge couplings for U(1)$'$ and U(1)$''$ respectively, and ϵ is the kinetic mixing parameter between U(1)$'$ and U(1)$_Y$. In this paper, we will mainly focus on cosmological features of the model. Thus, the parameters can be traded with relevant effective parameters $\{m_1, m_2, \Omega_{\rm DM}, r_1, \sigma_{\rm self1}, \sigma_{\rm self2}\}$, where $\Omega_{\rm DM}$ is fixed at 0.27 to yield the observed value and $\sigma_{\rm self1}$ ($\sigma_{\rm self2}$) denotes a self-scattering cross section of χ_1 (χ_2). We note that $\sigma_{\rm self1}$ (diagram II in Fig. 1) plays an important role in sharing the excessive kinetic energy of boosted χ_1 particles with the rest of their species and hence increasing the overall χ_1 temperature $T_1 = T_{\chi_1}$ [60]. In principle, the self-interaction of nonrelativistic χ_2 particles can also have an influence on perturbation evolution, but to focus on the main dynamics of χ_1 self-heating, we will neglect the contribution of $\sigma_{\rm self2}$. In fact, the self-interaction of χ_2 and diagram I in Fig. 1 are expected to be of similar sizes because both are mediated by the U(1)$''$ interaction. The self-interaction of χ_2 does not have to be strong, as long as $\Gamma_{\rm heat}$(diagram I) $> \Gamma_{\rm el}$(diagram III), in which case such nonstrong self-interaction of χ_2 does not affect the structure formation. Therefore, the parameters determining the most prominent features in cosmological simulation are $\{m_1, m_2, r_1, \sigma_{\rm self1}\}$.

3. Temperature evolution

The cosmological evolution for the number densities of χ_1, χ_2 and SM particles X, $n_{1,2,X}$ is governed by coupled Boltzmann equations as in Refs. [3,60], and will be discussed in detail in a companion paper [61]. Here, we focus on the temperature evolution of the light component χ_1.

After the decoupling of DM particles from the SM plasma (with temperature T), the $\bar{\chi}_2\chi_2 \to \bar{\chi}_1\chi_1$ annihilation (diagram I in Fig. 1) can leverage the mass gap $\delta m = m_2 - m_1$ to produce energetic χ_1 particles. If $\Gamma_{\rm self} > H$, the excessive kinetic energy ($\Gamma_{\rm heat} > \Gamma_{\rm el}$) is thermalized to increase the overall temperature of χ_1 particles (the heating-up period in Fig. 1). The evolution of its temperature T_1 is governed by

$$\dot{T}_1 \simeq -2HT_1 + \gamma_{\rm heat}T - 2\gamma_{\chi_1 X}(T_1 - T), \tag{1}$$

where the first term on the right-hand side represents the Hubble friction due to the expansion of the Universe, and the second is responsible for the self-heating with $\gamma_{\rm heat} \simeq 2n_2^2\langle\sigma v\rangle_{22\to 11}\delta m/\left(3n_1 T\right)$ [60]. Note that, although the larger mass difference δm leads to a higher temperature T_1 in general, it is closely associated with the relative number densities of χ_1 and χ_2 as well. The last term of Eq. (1) describes the energy exchange between χ_1 and the SM plasma with $\gamma_{\chi_1 X} \simeq \left(\delta E/T\right)n_X\langle\sigma v\rangle_{\chi_1 X}$, where δE is the change in χ_1 kinetic energy per elastic

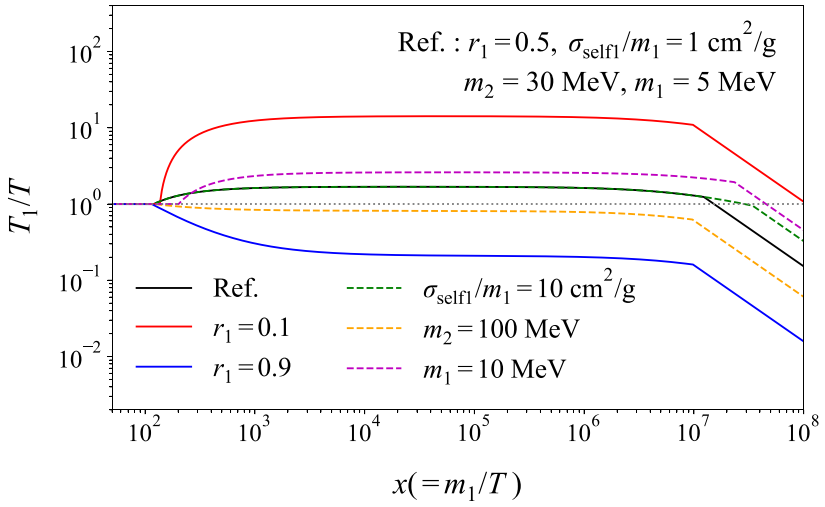

Fig. 2. Temperature evolution T_1 of dark matter χ_1 as a function of $x = m_1/T$ under various benchmark model parameters.

scattering and $\langle \sigma v \rangle_{\chi_1 X}$ is the thermally averaged scattering cross section of χ_1 off SM particles X.[1]

Figure 2 shows the evolution of T_1/T as a function of $x = m_1/T$ for a few selections of parameter sets by varying one parameter at a time with respect to a benchmark point ($r_1 = 0.5$, $\sigma_{\rm self1}/m_1 = 1$ cm^2/g, $m_2 = 30$ MeV, $m_1 = 5$ MeV). The results in Fig. 2 are exactly what was expected from the illustration in Fig. 1. Several important comments are in order. First, to boost the temperature T_1, a larger χ_2 density is favored ($r_1 \ll 1$). On the other hand, if the χ_2 density is smaller than χ_1 ($r_1 \to 1$), fewer energetic χ_1 particles are produced from the χ_2 annihilation. With only a small amount of extra energy available, it is not enough to heat a large portion of the relic χ_1 population, which leads to a lower T_1 temperature. Second, the self-interaction $\sigma_{\rm self1}/m_1$ determines the duration of the self-heating effect. For example, with an increase in $\sigma_{\rm self1}/m_1$ from 1 cm^2/g (black solid) to 10 cm^2/g (green dashed), the more prolonged time that T_1 is heated, and hence its temperature starts to fall much later. Finally, the self-heating is more sensitive to the combination of number density n_2^2/n_1 than the mass difference δm. An increase of m_2 from 30 MeV (black solid) to 100 MeV (orange dashed) leads to a large δm, but the number density n_2 drops as $n_2 \simeq \rho_2/m_2$ for nonrelativistic particles. As a result, the T_1 value for the $m_2 = 100$ MeV case is lower than that for the $m_2 = 30$ MeV case. Similarly, an increase of m_1 from 5 MeV (black solid) to 10 MeV (purple dashed) leads to a larger temperature due to the decreased number density n_1.

4. Perturbation evolution

We are now ready to derive the matter perturbation equations. We focus on the perturbations of χ_1 and χ_2 fluids; investigation of the perturbations of SM fluids is left for future work. We introduce the metric fluctuations in the Newtonian gauge as

$$ds^2 = -(1 + 2\Psi)dt^2 + (1 - 2\Phi)a(t)^2\delta_{ij}dx^i dx^j, \tag{2}$$

[1]Note that the temperature evolution of BDM models with the DM conversion has been studied in Ref. [60].

where $a(t)$ is a cosmological scale factor and Ψ and Φ denote scalar perturbations. Manipulating the standard procedure with the metric fluctuations and covariant derivatives of energy–momentum tensors [62], we derive the following coupled differential equations for the density perturbation (for the first time):

$$\frac{d\delta_2}{dt}+\frac{\theta_2}{a}-3\frac{d\Phi}{dt}=\frac{\langle\sigma v\rangle_{22\to 11}}{m_2\bar{\rho}_2}\Bigg(-\Psi(\bar{\rho}_2^2-\frac{\bar{\rho}_{2,\mathrm{eq}}^2}{\bar{\rho}_{1,\mathrm{eq}}^2}\bar{\rho}_1^2)-\bar{\rho}_2^2\delta_2 + \frac{\bar{\rho}_{2,\mathrm{eq}}^2}{\bar{\rho}_{1,\mathrm{eq}}^2}\bar{\rho}_1^2(2\delta_{2,\mathrm{eq}}-\delta_2-2\delta_{1,\mathrm{eq}}+2\delta_1)\Bigg), \tag{3}$$

$$\frac{d\theta_2}{dt}+H\theta_2+\frac{\nabla^2\Psi}{a}=\frac{\langle\sigma v\rangle_{22\to 11}}{m_2\bar{\rho}_2}\frac{\bar{\rho}_{2,\mathrm{eq}}^2}{\bar{\rho}_{1,\mathrm{eq}}^2}\bar{\rho}_1^2(\theta_1-\theta_2), \tag{4}$$

$$\begin{aligned}\frac{d\delta_1}{dt}+\frac{\theta_1}{a}-3\frac{d\Phi}{dt}=&-\frac{\langle\sigma v\rangle_{22\to 11}}{m_2\bar{\rho}_1}\Bigg(-\Psi(\bar{\rho}_2^2-\frac{\bar{\rho}_{2,\mathrm{eq}}^2}{\bar{\rho}_{1,\mathrm{eq}}^2}\bar{\rho}_1^2)-\bar{\rho}_2^2(2\delta_2-\delta_1)\\ &+\frac{\bar{\rho}_{2,\mathrm{eq}}^2}{\bar{\rho}_{1,\mathrm{eq}}^2}\bar{\rho}_1^2(2\delta_{2,\mathrm{eq}}+\delta_1-2\delta_{1,\mathrm{eq}})\Bigg)\\ &+\frac{\langle\sigma v\rangle_{11\to XX}}{m_1\bar{\rho}_1}\Bigg(-\Psi(\bar{\rho}_1^2-\bar{\rho}_{1,\mathrm{eq}}^2)-\bar{\rho}_1^2\delta_1+\bar{\rho}_{1,\mathrm{eq}}(2\delta_{1,\mathrm{eq}}-\delta_1)\Bigg),\end{aligned} \tag{5}$$

$$\frac{d\theta_1}{dt}+H\theta_1+\frac{\nabla^2\Psi}{a}+c_{s,1}^2\frac{\nabla^2\delta_1}{a}=\frac{\langle\sigma v\rangle_{22\to 11}}{m_2\bar{\rho}_1}\bar{\rho}_2^2(\theta_2-\theta_1), \tag{6}$$

where ρ_α, $\bar{\rho}_\alpha$, $\delta_\alpha=\delta\rho_\alpha/\bar{\rho}_\alpha$, and θ_α represent energy densities, background energy densities, density contrasts, and velocity divergence fields, respectively.

Equations (3)–(6) reproduce the perturbed Boltzmann equations for the CDMs in the vanishing nongravitational interaction limit. The source terms on the right-hand side of the Euler equations in Eqs. (4), (6) describe the momentum transfers between the χ_2 and χ_1 particles that are proportional to the scattering rate, $\langle\sigma v\rangle_{22\to 11}$, and to the difference in χ_2 and χ_1 velocities, $\theta_2-\theta_1$. As expected, the scattering tries to make the χ_1 particles move faster for large $\langle\sigma v\rangle_{22\to 11}$. The last term on the left-hand side of Eq. (6) describes the pressure of χ_1 DM as a consequence of the temperature increase from the self-heating effect. Given the χ_1 temperature evolution in Eq. (1), the sound speed of the χ_1 fluid is computed from [63]

$$c_{s,1}^2=\frac{T_1}{m_1}\Big(1-\frac{1}{3}\frac{\partial\ln T_1}{\partial\ln a}\Big), \tag{7}$$

which is valid if T_1 is much smaller than its mass m_1.

On the other hand, since the χ_2 particles behave like pressureless CDM, we neglect the pressure term for χ_2 in our analysis. Finally, the evolution of gravity perturbations, Ψ and Φ, are governed by the space–time and space–space components of perturbed Einstein equations. In the presence of the anisotropic tensors due to the contributions from photons and neutrinos, in general, $\Psi\neq\Phi$, which we consider properly in our study.

We have implemented the above background and perturbation equations inside the Cosmic Linear Anisotropy Solving System, `CLASS` (v3.2) [64]. This implementation is based on an effective theory of structure formation [65] to parameterize various DM models. When modifying the code, we map χ_2 to CDM and χ_1 to IDM, where IDM denotes an interacting DM species, disabling irrelevant interactions (see Refs. [65,66] for an analogous strategy). We use

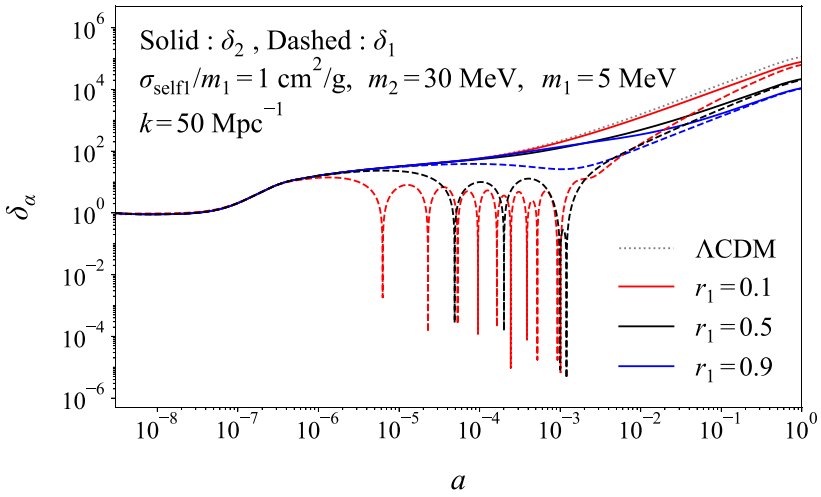

Fig. 3. Evolution of dark matter density perturbations under various benchmark model parameters.

the following parameters based on Planck 2018 [67] ΛCDM parameters, $\{\Omega_\Lambda, \Omega_m, \Omega_b, h, \sigma_8\} = \{0.6889, 0.3111, 0.049, 0.6766, 0.8102\}$ for the analysis in the rest of this paper.

Figure 3 shows the evolution of density contrasts δ_1 (dashed) and δ_2 (solid) as a function of a scale factor a for a fixed mode $k = 50\ {\rm Mpc}^{-1}$. The δ_2 value goes through a significant change around the time of matter–radiation equality, $a \sim \mathcal{O}(10^{-4})$. In the single-component DM limit of $r_1 \simeq 0$, the matter energy density is dominated by χ_2, and the evolution of δ_2 resembles that of the single CDM model. This picture starts to deviate as r_1 increases, where the annihilation cross section $\langle\sigma v\rangle_{22\to 11}$ becomes large. It turns out that, in this case, δ_2 experiences stronger friction due to the disappearance of the gravitational potential well from the χ_2 annihilation, and hence its overall growth is suppressed.

δ_1 exhibits oscillatory behavior that hinders the growth of matter perturbations, even in the deep radiation era. As $r_1 \to 0$, the temperature T_1 increases, enhancing the pressure due to the self-heating over gravity and causing oscillations similar to SM baryon acoustic oscillations. However, with rising r_1, T_1 decreases, so that the gravitational force starts to balance out with the pressure, causing δ_1 to stop oscillating.

All the features described above are somewhat less significant for a small-k mode. The evolution of δ_2 is nearly the same as that of CDM and is unaffected by the ratio parameter r_1. There is a slight suppression in δ_1 in the limit $r_1 \ll 1$, but it does not show oscillatory behavior.

5. Linear power spectrum

With the density perturbations δ_1 and δ_2 obtained above, the linear matter power spectrum can be readily computed with `CLASS` [64], as shown in Fig. 4. In the WDM scenarios, the particles are in a relativistic state during the deep radiation epoch, which causes the density perturbations of the particles to be suppressed at the scale below the free-streaming length. Analogously, in the multicomponent model, the power spectrum is suppressed as a result of the self-heating effect through self-interaction of χ_1. Therefore, the CDM candidate χ_1 at the MeV mass scale behaves like WDM (at the keV mass scale) via interactions between dark matter particles. Similarly, the oscillatory behavior at $k \gtrsim 100\ h/{\rm Mpc}$ (often known as the characteristic of WDM) is due to the competition between the gravitational potential and the pressure of the χ_1 fluid.

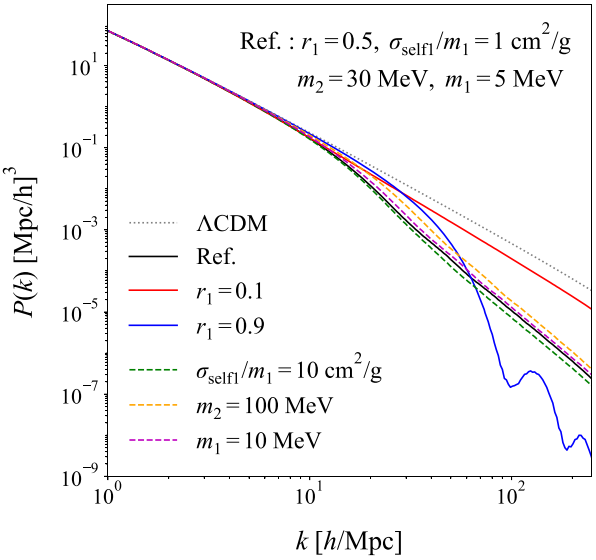

Fig. 4. Linear matter power spectrum for various choices of parameters.

The suppression scale k depends on r_1. For $k\langle 20\ h/\text{Mpc}$, the suppression becomes maximal at an intermediate value of r_1, and then the power spectrum increases toward the ΛCDM case as r_1 increases; e.g. $r_1 \sim 0.5$ leads to the lowest power spectrum below $k \sim 20\ h/\text{Mpc}$ for the reference choice in Fig. 4. On the other hand, for $k\rangle 100\ h/\text{Mpc}$, the larger r_1 leads to a lower power spectrum because there are too many χ_1 particles with self-interaction in the large-r_1 limit.

Note that the elastic scattering between χ_1 and χ_2 and between χ_1 and photons contributes to the right-hand sides of Eqs. (4) and (6), respectively. The χ_1–photon elastic scattering suppresses the power spectrum as the χ_1 perturbations are suppressed on scales that enter the horizon before the kinetic decoupling [68,69]. Such effects appear at $k \gtrsim 500\ h/\text{Mpc}$ for a large value of r_1 in our power spectrum, which we find negligible.

6. *N*-body simulation

The simulation of two-component DM [] is carried out with `GADGET-3` [70,71]. To provide an initial input, we use the Planck 2018 [67] ΛCDM parameters. The dimensions of a periodic comoving box are set at $L = 3\ h^{-1}$Mpc with a total of $N_{\rm tot} = 128^3$ DM clumps. The numbers of χ_1 and χ_2 clumps are set at $N_{\rm tot} r_1$ and $N_{\rm tot}(1 - r_1)$, respectively. The simulation runs from a redshift of $z = 49$ to $z = 0$. Using the linear matter power spectrum from `CLASS` at $z = 0$, we apply a backward method [72] to derive the spectrum at $z = 49$ for generating initial density perturbations via second-order Lagrangian perturbation theory (2LPT) [73].

The light component, χ_1, experiences elastic self-interactions. We model these interactions using the Monte Carlo (MC) technique, which is a standard method for simulating self-interacting DM in large-scale N-body simulations [74–78]. The MC method helps to statistically determine the likelihood of interactions between χ_1 clumps based on various factors like local density and velocity. The probability of a self-interaction between two clumps is influenced by the local density of the target clump, the relative velocity between the two clumps, and the cross section of their interaction. The interaction is kinematically constrained so that only allowed configurations of outgoing clumps are considered. We assume that the outgoing

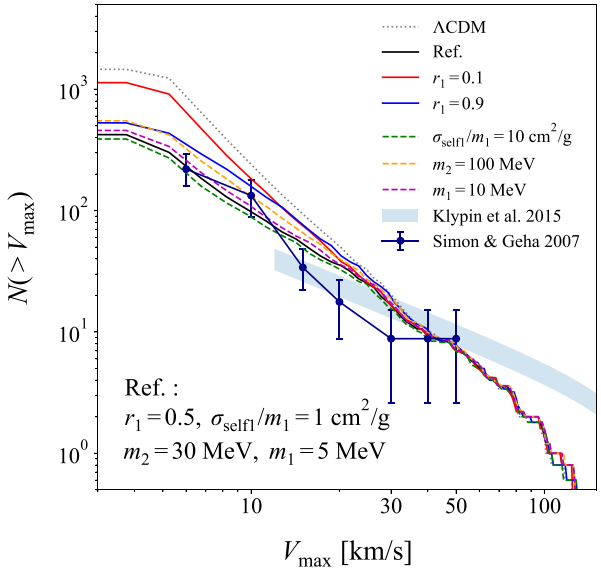

Fig. 5. The number of accumulated sub-halos as a function of the maximum circular velocity for various parameters in the two-component dark matter model.

clumps scatter isotropically; i.e. their distribution is uniform in all directions, and the interaction cross section is assumed to be independent of the scattering angle. The self-interactions of the heavy DM component, χ_2, are excluded from the simulation to focus on the dynamics of χ_1. Additionally, the simulation ignores the annihilation of χ_2 into χ_1 particles, as this process has a much lower rate compared to the expansion of the Universe in its late stages. This simplification allows the simulation to concentrate on the more dominant interactions within the χ_1 component for a clearer view of the main behavior of self-interacting DM without introducing unnecessary complexity from weaker or less relevant processes. See Ref. [61] for more details.

To extract halo properties, we use the friends-of-friends (FOF) method to identify groups of DM clumps that surpass the virial overdensity. The linking length of the FOF algorithm is 0.2. We use $3.56 \times 10^7 M_\odot$ and $2.22 \times 10^7 M_\odot$ for the minimum masses of the halos and sub-halos, respectively. These values are determined by the size of the periodic comoving box and the number of DM clumps in our simulation [73].[2]

Among many interesting quantities, we focus on the maximum velocity of sub-halos, i.e. MCVF, which is related to the mass scale of the sub-halos. Figure 5 shows the number of accumulated sub-halos ($N(\rangle V_{\rm max})$) as a function of their maximum velocity ($V_{\rm max}$) for various selections of parameters with respect to the reference. A larger value of $V_{\rm max}$ implies heavier sub-halos. Our results show that, in the multicomponent scenario, the number of sub-halos is reduced compared to the ΛCDM simulation, mitigating the so-called missing satellite problem [79,80]. Baryonic effects are also known to lower the magnitude of MCVF [81,82]. However, such effects may not be strong enough for experimental data, which motivates the inclusion of WDM additionally [81,82]. Our two-component dark matter is similar in the sense that the light CDM component plays the role of WDM in the N-body simulation.

[2]More details on the N-body simulation will be given in Ref. [61].

7. Conclusion and outlook

In this paper, we have introduced a model with two-component CDM, where the lighter component behaves like WDM. For the first time, we have investigated the temperature evolution, density perturbation, linear power spectrum, and maximum circular velocity function via N-body simulation. Such various cosmological implications provide a crucial input to particle physics experiments. For example, performing a simple fit to the MCVF in Fig. 5 returns a benchmark reference model, with which one can compute the expected event rates (via the elastic scattering process III in Fig. 1) per year at terrestrial experiments such as Super-Kamiokande [83], XENONnT [84], and JUNO [85]. Further discussion is needed for the full investigation of cosmological and phenomenological implications of boosted dark matter, including the nonlinear power spectrum, halo profile, baryonic effect, and gravitational wave signals; this is beyond the scope of the current study and will be performed elsewhere.

Acknowledgments

We thank Donghui Jeong, Jinn-Ouk Gong, and Chang Sub Shin for useful discussion. The work is supported by a National Research Foundation of Korea grant funded by the Korea government (MSIT) [NRF-2021R1C1C1005076 (J.H.K., S.H.L.), NRF-2019R1C1C1005073, RS-2024-00356960 (J.C.P.)]. K.K. is supported in part by US DOE DE-SC0024407 and University of Kansas General Research Fund allocation.

Funding

Open Access funding: SCOAP[3].

References

[1] J. Cooley et al., arXiv:2209.07426 [hep-ph] [Search inSPIRE].
[2] F. D'Eramo and J. Thaler, J. High Energy Phys. **1006**, 109 (2010) [arXiv:1003.5912 [hep-ph]] [Search inSPIRE].
[3] G. Belanger and J.-C. Park, J. Cosmol. Astropart. Phys. **1203**, 038 (2012) [arXiv:1112.4491 [hep-ph]] [Search inSPIRE].
[4] L. Perivolaropoulos and F. Skara, New Astron. Rev. **95**, 101659 (2022) [arXiv:2105.05208 [astro-ph.CO]] [Search inSPIRE].
[5] H. Huang, H.-Y. Schive, and T. Chiueh, Mon. Not. R. Astron. Soc. **522**, 515 (2023) [arXiv:2212.14288 [astro-ph.CO]] [Search inSPIRE].
[6] A. V. Maccio, O. Ruchayskiy, A. Boyarsky, and J. C. Munoz-Cuartas, Mon. Not. R. Astron. Soc. **428**, 882 (2013) [arXiv:1202.2858 [astro-ph.CO]] [Search inSPIRE].
[7] G. Parimbelli, G. Scelfo, S. K. Giri, A. Schneider, M. Archidiacono, S. Camera, and M. Viel, J. Cosmol. Astropart. Phys. **2112**, 044 (2021) [arXiv:2106.04588 [astro-ph.CO]] [Search inSPIRE].
[8] A. Boyarsky, J. Lesgourgues, O. Ruchayskiy, and M. Viel, J. Cosmol. Astropart. Phys. **2009**, 012 (2009).
[9] A. V. Macciò, O. Ruchayskiy, A. Boyarsky, and J. C. Muñoz-Cuartas, Mon. Not. R. Astron. Soc. **428**, 882 (2012).
[10] D. Anderhalden, J. Diemand, G. Bertone, A. V. Macciò, and A. Schneider, J. Cosmol. Astropart. Phys. **2012**, 047 (2012).
[11] M. V. Medvedev, Phys. Rev. Lett. **113**, 071303 (2014) [arXiv:1305.1307 [astro-ph.CO]] [Search inSPIRE].
[12] K. Todoroki and M. V. Medvedev, Mon. Not. R. Astron. Soc. **483**, 3983 (2019) [arXiv:1711.11078[astro-ph.CO]] [Search inSPIRE].
[13] K. Todoroki and M. V. Medvedev, Mon. Not. R. Astron. Soc. **483**, 4004 (2019) [arXiv:1711.11085 [astro-ph.CO]] [Search inSPIRE].
[14] K. Todoroki and M. V. Medvedev, Mon. Not. R. Astron. Soc. **510**, 4249 (2022) [arXiv:2003.11096 [astro-ph.CO]] [Search inSPIRE].

[15] A. Garzilli, A. Magalich, O. Ruchayskiy, and A. Boyarsky, Mon. Not. R. Astron. Soc. **502**, 2356 (2021) [arXiv:1912.09397 [astro-ph.CO]] [Search inSPIRE].
[16] B. Villasenor, B. Robertson, P. Madau, and E. Schneider, Phys. Rev. D **108**, 023502 (2023) [arXiv:2209.14220 [astro-ph.CO]] [Search inSPIRE].
[17] Y. Hochberg, Y. Zhao, and K. M. Zurek, Phys. Rev. Lett. **116**, 011301 (2016) [arXiv:1504.07237 [hep-ph]] [Search inSPIRE].
[18] K. Schutz and K. M. Zurek, Phys. Rev. Lett. **117**, 121302 (2016) [arXiv:1604.08206[hep-ph]] [Search inSPIRE].
[19] Y. Hochberg, Y. Kahn, M. Lisanti, K. M. Zurek, A. G. Grushin, R. Ilan, S. M. Griffin, Z.-F. Liu, S. F. Weber, and J. B. Neaton, Phys. Rev. D **97**, 015004 (2018) [arXiv:1708.08929 [hep-ph]] [Search inSPIRE].
[20] S. Knapen, T. Lin, M. Pyle, and K. M. Zurek, Phys. Lett. B **785**, 386 (2018) [arXiv:1712.06598 [hep-ph]] [Search inSPIRE].
[21] Y. Hochberg, I. Charaev, S.-W. Nam, V. Verma, M. Colangelo, and K. K. Berggren, Phys. Rev. Lett. **123**, 151802 (2019) [arXiv:1903.05101 [hep-ph]] [Search inSPIRE].
[22] D. Kim, J.-C. Park, K. C. Fong, and G.-H. Lee, arXiv:2002.07821 [hep-ph][Search inSPIRE].
[23] L. Barak et al., Phys. Rev. Lett. **125**, 171802 (2020) [arXiv:2004.11378[astro-ph.CO]] [Search inSPIRE].
[24] Y. Hochberg, B. V. Lehmann, I. Charaev, J. Chiles, M. Colangelo, S. W. Nam, and K. K. Berggren, Phys. Rev. D **106**, 112005 (2022) [arXiv:2110.01586 [hep-ph]] [Search inSPIRE].
[25] K. Agashe, Y. Cui, L. Necib, and J. Thaler, J. Cosmol. Astropart. Phys. **1410**, 062 (2014) [arXiv:1405.7370 [hep-ph]] [Search inSPIRE].
[26] J. Berger, Y. Cui, and Y. Zhao, J. Cosmol. Astropart. Phys. **1502**, 005 (2015) [arXiv:1410.2246 [hep-ph]] [Search inSPIRE].
[27] K. Kong, G. Mohlabeng, and J.-C. Park, Phys. Lett. B **743**, 256 (2015) [arXiv:1411.6632 [hep-ph]] [Search inSPIRE].
[28] J. F. Cherry, M. T. Frandsen, and I. M. Shoemaker, Phys. Rev. Lett. **114**, 231303 (2015) [arXiv:1501.03166 [hep-ph]] [Search inSPIRE].
[29] L. Necib, J. Moon, T. Wongjirad, and J. M. Conrad, Phys. Rev. D **95**, 075018 (2017) [arXiv:1610.03486[hep-ph]] [Search inSPIRE].
[30] H. Alhazmi, K. Kong, G. Mohlabeng, and J.-C. Park, J. High Energy Phys. **1704**, 158 (2017) [arXiv:1611.09866[hep-ph]] [Search inSPIRE].
[31] D. Kim, J.-C. Park, and S. Shin, Phys. Rev. Lett. **119**, 161801 (2017) [arXiv:1612.06867 [hep-ph]] [Search inSPIRE].
[32] C. Kachulis et al., Phys. Rev. Lett. **120**, 221301 (2018) [arXiv:1711.05278 [hep-ex]] [Search inSPIRE].
[33] G. F. Giudice, D. Kim, J.-C. Park, and S. Shin, Phys. Lett. B **780**, 543 (2018) [arXiv:1712.07126[hep-ph]] [Search inSPIRE].
[34] A. Chatterjee, A. De Roeck, D. Kim, Z. Gh. Moghaddam, J.-C. Park, S. Shin, L. H. Whitehead, and J. Yu, Phys. Rev. D **98**, 075027 (2018) [arXiv:1803.03264 [hep-ph]] [Search inSPIRE].
[35] D. Kim, K. Kong, J.-C. Park, and S. Shin, J. High Energy Phys. **1808**, 155 (2018) [arXiv:1804.07302[hep-ph]] [Search inSPIRE].
[36] T. Bringmann and M. Pospelov, Phys. Rev. Lett. **122**, 171801 (2019) [arXiv:1810.10543 [hep-ph]] [Search inSPIRE].
[37] Y. Ema, F. Sala, and R. Sato, Phys. Rev. Lett. **122**, 181802 (2019) [arXiv:1811.00520 [hep-ph]] [Search inSPIRE].
[38] C. Ha et al., Phys. Rev. Lett. **122**, 131802 (2019) [arXiv:1811.09344[astro-ph.IM]] [Search inSPIRE].
[39] D. Kim, J.-C. Park, and S. Shin, Phys. Rev. D **100**, 035033 (2019) [arXiv:1903.05087 [hep-ph]] [Search inSPIRE].
[40] L. Heurtier, D. Kim, J.-C. Park, and S. Shin, Phys. Rev. D **100**, 055004 (2019) [arXiv:1905.13223 [hep-ph]] [Search inSPIRE].
[41] J. Berger, Y. Cui, M. Graham, L. Necib, G. Petrillo, D. Stocks, Y.-T. Tsai, and Y. Zhao, Phys. Rev. D **103**, 095012 (2021) [arXiv:1912.05558 [hep-ph]] [Search inSPIRE].
[42] D. Kim, P. A. N. Machado, J.-C. Park, and S. Shin, J. High Energy Phys. **2007**, 057 (2020) [arXiv:2003.07369[hep-ph]] [Search inSPIRE].

[43] A. De Roeck, D. Kim, Z. Gh. Moghaddam, J.-C. Park, S. Shin, and L. H. Whitehead, J. High Energy Phys. **2011**, 043 (2020) [arXiv:2005.08979 [hep-ph]] [Search inSPIRE].
[44] Q.-H. Cao, R. Ding, and Q.-F. Xiang, Chin. Phys. C **45**, 045002 (2021) [arXiv:2006.12767 [hep-ph]] [Search inSPIRE].
[45] Y. Jho, J.-C. Park, S. C. Park, and P.-Y. Tseng, Phys. Lett. B **811**, 135863 (2020) [arXiv:2006.13910 [hep-ph]] [Search inSPIRE].
[46] H. Alhazmi, D. Kim, K. Kong, G. Mohlabeng, J.-C. Park, and S. Shin, J. High Energy Phys. **2105**, 055 (2021) [arXiv:2006.16252 [hep-ph]] [Search inSPIRE].
[47] Y. Jho, J.-C. Park, S. C. Park, and P.-Y. Tseng, arXiv:2101.11262 [hep-ph] [Search inSPIRE].
[48] N. F. Bell, J. B. Dent, B. Dutta, S. Ghosh, J. Kumar, J. L. Newstead, and I. M. Shoemaker, Phys. Rev. D **104**, 076020 (2021) [arXiv:2108.00583 [hep-ph]] [Search inSPIRE].
[49] W. Wang, L. Wu, W.-N. Yang, and B. Zhu, Phys. Rev. D **107**, 073002 (2023) [arXiv:2111.04000 [hep-ph]] [Search inSPIRE].
[50] J.-W. Wang, A. Granelli, and P. Ullio, Phys. Rev. Lett. **128**, 221104 (2022) [arXiv:2111.13644[astro-ph.HE]] [Search inSPIRE].
[51] X. Cui et al., Phys. Rev. Lett. **128**, 171801 (2022) [arXiv:2112.08957 [hep-ex]] [Search inSPIRE].
[52] R. Xu et al., Phys. Rev. D **106**, 052008 (2022) [arXiv:2201.01704 [hep-ex]] [Search inSPIRE].
[53] N. Y. Agafonova et al., J. Cosmol. Astropart. Phys. **2307**, 067 (2023) [arXiv:2305.00112 [astro-ph.IM]] [Search inSPIRE].
[54] G. Adhikari et al., Phys. Rev. Lett. **131**, 201802 (2023) [arXiv:2306.00322 [hep-ex]] [Search inSPIRE].
[55] A. Guha and J.-C. Park, J. Cosmol. Astropart. Phys. **2407**, 074 (2024) [arXiv:2401.07750[hep-ph]] [Search inSPIRE].
[56] B. Dutta, W.-C. Huang, D. Kim, J. L. Newstead, J.-C. Park, and I. S. Ali, Phys. Rev. Lett. **133**, 161801 (2024) [arXiv:2402.04184 [hep-ph]] [Search inSPIRE].
[57] X. Shang et al., Phys. Rev. Lett. **133**, 101805 (2024) [arXiv:2403.08361 [hep-ex]] [Search inSPIRE].
[58] R. Xu et al., arXiv:2403.20276 [hep-ex] [Search inSPIRE].
[59] K. Choi and J.-C. Park, arXiv:2409.05646 [hep-ph] [Search inSPIRE].
[60] A. Kamada, H. J. Kim, J.-C. Park, and S. Shin, J. Cosmol. Astropart. Phys. **2210**, 052 (2022) [arXiv:2111.06808 [hep-ph]] [Search inSPIRE].
[61] J. H. Kim, K. Kong, S. H. Lim, and J.-C. Park, arXiv:2410.05382 [hep-ph] [Search inSPIRE].
[62] D. Baumann, Cosmology (Cambridge University Press, Cambridge, UK, 2022). doi:10.1017/9781108937092
[63] N. Becker, D. C. Hooper, F. Kahlhoefer, J. Lesgourgues, and N. Schöneberg, J. Cosmol. Astropart. Phys. **2102**, 019 (2021) [arXiv:2010.04074 [astro-ph.CO]] [Search inSPIRE].
[64] D. Blas, J. Lesgourgues, and T. Tram, J. Cosmol. Astropart. Phys. **1107**, 034 (2011) [arXiv:1104.2933 [astro-ph.CO]] [Search inSPIRE].
[65] F.-Y. Cyr-Racine, K. Sigurdson, J. Zavala, T. Bringmann, M. Vogelsberger, and C. Pfrommer, Phys. Rev. D **93**, 123527 (2016) [arXiv:1512.05344 [astro-ph.CO]] [Search inSPIRE].
[66] S. Bansal, J. H. Kim, C. Kolda, M. Low, and Y. Tsai, J. High Energy Phys. **2205**, 050 (2022) [arXiv:2110.04317 [hep-ph]] [Search inSPIRE].
[67] N. Aghanim et al., Astron. Astrophys. **641**, A6 (2020); **652**, C4 (2021) [erratum][arXiv:1807.06209[astro-ph.CO]] [Search inSPIRE].
[68] K.-Y. Choi, J.-O. Gong, and C. S. Shin, Phys. Rev. Lett. **115**, 211302 (2015) [arXiv:1507.03871 [astro-ph.CO]] [Search inSPIRE].
[69] A. L. Erickcek, Phys. Rev. D **92**, 103505 (2015) [arXiv:1504.03335 [astro-ph.CO]] [Search inSPIRE].
[70] V. Springel, Mon. Not. R. Astron. Soc. **364**, 1105 (2005).
[71] V. Springel, J. Wang, M. Vogelsberger, A. Ludlow, A. Jenkins, A. Helmi, J. F. Navarro, C. S. Frenk, and S. D. M. White, Mon. Not. R. Astron. Soc. **391**, 1685 (2008).
[72] R. E. Angulo and O. Hahn, arXiv:2112.05165 [astro-ph.CO] [Search inSPIRE].
[73] M. Crocce, S. Pueblas, and R. Scoccimarro, Mon. Not. R. Astron. Soc. **373**, 369 (2006).
[74] M. Rocha, A. H. G. Peter, J. S. Bullock, M. Kaplinghat, S. Garrison-Kimmel, J. Onorbe, and L. A. Moustakas, Mon. Not. R. Astron. Soc. **430**, 81 (2013) [arXiv:1208.3025 [astro-ph.CO]] [Search inSPIRE].

[75] K.-J. Ahn and P. R. Shapiro, Mon. Not. R. Astron. Soc. **363**, 1092 (2005) [arXiv:astro-ph/0412169][Search inSPIRE].
[76] P. Colín, V. Avila-Reese, O. Valenzuela, and C. Firmani, Astrophys. J. **581**, 777 (2002).
[77] B. Moore, S. Gelato, A. Jenkins, F. R. Pearce, and V. Quilis, Astrophys. J. Lett. **535**, L21 (2000) [arXiv:astro-ph/0002308] [Search inSPIRE].
[78] D. N. Spergel and P. J. Steinhardt, Phys. Rev. Lett. **84**, 3760 (2000) [arXiv:astro-ph/9909386] [Search INSPIRE].
[79] J. D. Simon and M. Geha, Astrophys. J. **670**, 313 (2007).
[80] A. Klypin, I. Karachentsev, D. Makarov, and O. Nasonova, Mon. Not. R. Astron. Soc. **454**, 1798 (2015).
[81] M. R. Lovell, V. Gonzalez-Perez, S. Bose, A. Boyarsky, S. Cole, C. S. Frenk, and O. Ruchayskiy, Mon. Not. R. Astron. Soc. **468**, 2836 (2017) [arXiv:1611.00005 [astro-ph.GA]] [Search inSPIRE].
[82] S. Y. Kim and A. H. G. Peter, arXiv:2106.09050 [astro-ph.GA][Search inSPIRE].
[83] Y. Fukuda et al., Nucl. Instrum. Meth. A **501**, 418 (2003).
[84] E. Aprile et al., Eur. Phys. J. C **77**, 881 (2017) [arXiv:1708.07051 [astro-ph.IM]] [Search inSPIRE].
[85] A. Abusleme et al., Prog. Part. Nucl. Phys. **123**, 103927 (2022) [arXiv:2104.02565 [hep-ex]] [Search inSPIRE].